International Research Journal of Mathematics, Engineering and IT
Vol. 3, Issue 6, June 2016 IF- 3.563 ISSN: (2349-0322)
© Associated Asia Research Foundation (AARF)
Website: www.aarf.asia Email : editor@aarf.asia , editoraarf@gmail.com

THE EFFECT OF THERMOPHORESIS ON CONVECTIVE HEAT AND MASS TRANSFER FLOW PAST A STRETCHING SHEET WITH SORET AND DUFOUR EFFECTS

K. Madhu Sudhana[1], B. Sreenivasa Reddy[2], M. Sreedhar Babu[2]

[1]Dept. of Mathematics, RGU I II T, R.K. Valley,Vempalli(m),Kadapa(d), AP, India.

[2]Asst.Professor, Dept. of Mathematics, Yogi Vemana University, Kadapa, AP, India.

ABSTRACT

Heat and mass transfer characteristics of an unsteady MHD boundary layer flow through porous medium over stretching sheet in the presence of Thermo-Diffusion and Diffusion-Thermo effects with thermophoresis, thermal radiation and non-uniform heat source/sink is discussed in this article. The transformed conservation equations are solved numerically subject to the boundary conditions using an optimized, extensively validated, variational finite element analysis. The numerical code is validated with previous studies. The influence of important non-dimensional parameters, namely Suction parameter (f_w), Magnetic parameter (M), Unsteadiness parameter (α), Soret parameter (Sr), Dufour parameter (Du) and thermophoretic parameter (τ) on velocity, temperature and concentration fields as well as Skin-friction coefficient, Nusselt number and Sherwood number are examined in detail and the results are shown in graphically and in tabular form to know the physical importance of the problem.

Keywords: Streching sheet;Duflour effects,Thermophoresis;Heat sources/sink; Finite element method.

1. INTRODUCTION

The problem of two dimensional boundary layer flow, heat and mass transfer over a continuous stretching heated surface through porous medium finds numerous and wide range of applications in many engineering and manufacturing disciplines. For example, in a melt spinning

process, the extrudate from the die is generally drawn and simultaneously stretched into a sheet or filament, which is thereafter solidified through rapid quenching or gradual cooling by direct contact with water or chilled metal rolls. In fact, stretching will bring in a unidirectional orientation to the extrudate, thereby improving the quality of the final product considerably which greatly depends on the flow, heat and mass transfer mechanism. Glass blowing, extrusion process, melt-spinning, food-stuff processing, design of heat exchangers, wire and fiber coating, glass-fiber production, manufacture of plastic and rubber sheets, cooling of a large metallicplate in a bath and continuous casting are the other areas where this kind of problems has applications.

In industry, polymer sheets and filaments are manufactured by continuous extrusion of the polymer from a die. The thin polymer sheet constitutes a continuously moving surface with a non-uniform velocity through an ambient fluid. The problem of heat and mass transfer flow due to stretching sheet has been implemented on many flow situations. The problem of steady two-dimensional viscous incompressible fluid caused by a stretching sheet was first examined by Sikiadis [1]. The thermal behavior of the problem was experimentally verified by Tsou et al [2]. Crane [3] has studied the flow past a stretching plate by taking velocity varying linearly with a distance from a fixed point and this problem is the extension of Sikiadis [1]. Gupta et al. [4] have studied heat and mass transfer characteristics of stretching sheet with suction or blowing. Grubka and Bobba [5]studied the heat transfer characteristics over a continuous stretching surface with variable temperature. Ali [6]has investigated flow and heat transfer characteristics on a continuous stretching surface usingpower-law velocity and temperature distributions. Vajravelu [7] has analyzed the study of flow and heat transfer in saturated porous medium over an impermeable stretching sheet. Two cases have been discussed in this problem, (i) the sheet with prescribed sheet temperature (PST-case) and (ii) the sheet with prescribed wall heat flux (PHF-case).

In all the previous investigations, the effects thermal radiation and magnetic field on the flow and heat transfer have not been studied. It is well known that radiative heat transfer flow is very important in manufacturing industries for the design of reliable equipment's, nuclear plants, gas turbines and various propulsion devices for aircraft, missiles, satellites and space vehicles. Also, the effects of thermal radiation on forced and free convection flow are important in the content of space technology and process involving high temperature.Recent developments in hypersonic flights, missile reentry rocket combustion chambers, gas cooled nuclearreactors and power plants for inter planetary flight, have focused attention of researchers on thermal radiation

as a mode of energy transfer, and emphasize the need for inclusion of radiative transfer in these process. Magneto nanofluids have specific applications in biomedicine, optical modulators, magnetic cell separation, magneto-optical wavelength filters, silk float separation, nonlinear optical materials, hyperthermia, optical switches, drug delivery, optical gratings etc. A magnetic nanofluids has both the liquid and magnetic properties. The used magnetic field influences the suspended particles and reorganizes their concentration in the fluid regime which powerfully influences the heat transfer analysis of the flow. Magneto nanofluids are useful to guide the particles up the blood stream to a tumor with magnets. This is due to the fact that the magnetic nanoparticles are regarded more adhesive to tumor cells than non-malignant cells. Such particles absorb more power than micro particles in alternating current magnetic fields tolerable in humans i.e. for cancer therapy. Plumb et al. [8] was the first to examine the effect of horizontal cross-flow and radiation on natural convection from vertical heated surface in a saturated porous media. Recently, Pal D et.al [9] has discussed radiation effect on hydro magnetic Darcy-Forchheimer mixed convention flow over stretching sheet. Mansur and El-Shear [10] analyzed the effects of thermal radiation on magneto hydrodynamic natural convection flows in a fluid-saturated porous media. Pal [11] studied heat and mass transfer in stagnation-point flow toward a stretching sheet in the presence of buoyancy force and thermal radiation. Vajravelu and Rollins [12] studied heat transfer in electrically conducting fluid over a stretching sheet by taking into account of magnetic field only. Molla et al. [13] studied the effect of thermal radiation on a steady two-dimensional natural convection laminar flow of viscous incompressible optically thick fluid along a vertical flat plate with stream wise sinusoidal surface temperature. Abo-Eldahab and El-Gendy [14] investigated the problem of free convection heat transfer characteristics in an electrically conducting fluid near an isothermal sheet to study the combined effect of buoyancy and radiation in the presence of uniform transverse magnetic field.

In recent years, it is found that thermophoresis is a phenomenon has many practical applications in removing small particles from gas streams, in determining exhaust gas particle trajectories from combustion devices, and in studying the particulate material deposition on turbine blades. It has been found that thermophoresis is the dominant mass transfer mechanism in the modified chemical vapor deposition (MCVD) process as currently used in the fabrication of optical fiber performs. Thermophoretic deposition of radioactive particles is considered to be one of the important factors causing accidents in nuclear reactors. A number of analytical and experimental papers in thermophoretic heat and mass transfer have been communicated. Talbot

et al. [15] presented a seminal study, considering boundary layer flow with thermophoretic effects, which has become a benchmark for subsequent studies. Several authors, Duwairi and Damseh et al. [16] ,Damseh et al. [17] , Mahdy and Hady [18] , Liu et al. [19] , Postelnicu [20] ,Dinesh and Jayaraj [21] , Grosan et al. [22] ,Tsai and Huang [23] have investigated the effect of thermophoresis in vertical plate, micro-channel, horizontal plate and parallel plate.

As many industrially and environmentally relevant fluids are not pure, it is been suggested that more attention should be paid to convective phenomena which can occur in mixtures, but are not in common liquids such as air or water. Applications involving liquid mixtures include the costing of alloys, ground water pollutant migration and separation operations. In all of these situations, multi component liquids can undergo natural convection driven by buoyancy force resulting from simultaneous temperature and species gradients. In the case of binary mixtures, the species gradients can be established by the applied boundary conditions such as species rejection associated with alloys costing, or can be induced by transport mechanism such as Soret (thermo) diffusion. In the case of Soret diffusion, species gradients are established in an otherwise uniform concentration mixture in accordance with Onsager reciprocal relationship. Thermal-diffusion known as the Soret effect takes place and as a result a mass fraction distribution is established in the liquid layer. The sense of migration of the molecular species is determined by the sign of Soret coefficient. Soret and Dufour effects are very significant in both Newtonian and non-Newtonian fluids when density differences exist in flow regime. The thermo-diffusion (Soret) effect is corresponds to species differentiation developing in an initial homogeneous mixture submitted to a thermal gradient and the diffusion-thermo (Dufour) effect corresponds to the heat flux produced by a concentration gradient. Usually, in heat and mass transfer problems the variation of density with temperature and concentration give rise to a combined buoyancy force under natural convection and hence the temperature and concentration will influence the diffusion and energy of the species. Many papers are found in literature on Soret and Dufour effects on different geometries. Dulal Pal et al.[24] has studied MHD non-Darcian mixed convection heat and mass transfer over a non-linear stretching sheet with Soret and Dufour effects and chemical reaction. MHD mixed convection flow with Soret and Dufour effects past a vertical plate embedded in porous medium was studied by Makinde. O.D [25]. Reddy P.S et al. [26] has presented finite element solution to the heat and mass transfer flow past a cylindrical annulus with Soret and Dufour effects. Recently, Chamkha A.J et al. [27] has studied the influence of Soret and Dufour effects on unsteady heat and mass

transfer flow over a rotating vertical cone and they suggested that temperature and concentration fields are more influenced with the values of Soret and Dufour parameter.

In all the above studies the physical situation is related to the process of uniform stretching sheet. For the development of more physically realistic characterization of the flow configuration it is very useful to introduce unsteadiness into the flow, heat and mass transfer problems. The working fluid heat generation or absorption effects are very crucial in monitoring the heat transfer in the regions, heat removal from nuclear fuel debris, underground disposal of radioactive waste material, storage of food stuffs, exothermic chemical reactions and dissociating fluids in packed-bed reactors. This heat source can occurs in the form of a coil or battery. Very few studies have been found in literature on unsteady boundary flows over a stretching sheet by taking heat generation/absorption into the account. Wang CY [28] was first studied the unsteady boundary layer flow of a liquid film over a stretching sheet. Later, Elbashbeshy and Bazid [29] have presented the heat transfer over an unsteady stretching surface. Tsai et.al [30] has discussed flow and heat transfer characteristics over an unsteady stretching surface by taking heat source into the account. Ishak et al [31] analyzed the effect of prescribed wall temperature on heat transfer flow over an unsteady stretching permeable surface. Is hack [32] has presented unsteady MHD flow and heat transfer behavior over a stretching plate. Recently, Dulal pal [33] has described the analysis of flow and heat transfer over an unsteady stretching surface with non-uniform heat source/sink and thermal radiation. Dulal pal et al. [34] have presented MHD non-Darcian mixed convection heat and mass transfer over a non- linear stretching sheet with Soret–Dufour effects, heat source/sink and chemical reaction

To the author knowledge no studies have been made to analyze the combined influence of Soret and Dufour effects on unsteady heat and mass transfer flow of a viscous incompressible electrically conducting fluid over a stretching sheet with thermal radiation, non-uniform heat source/sink and thermophoresis particle deposition. Hence, this problem is addressed in this paper. The conservation of mass, momentum, energy and diffusion equations were transformed into a two-point boundary value problem. In this article, we employ an extensively validated, highly efficient, variational finite-element method to study the effect of unsteadiness on heat and mass transfer flow in a porous medium past a semi-infinite stretching sheet. The problem presented here has many practical applications, such as, technological, manufacturing industries, MHD generators, plasma studies, nuclear reactors, geothermal energy extractions and polymer extrusion. Non-linear stretching velocity, surface temperature and surface concentration are

considered in the present paper. The nonlinearity of the basic equations and additional mathematical difficulties associated with it, have led to the use of numerical method.

2. FORMULATION OF THE PROBLEM

Consider a two-dimensional unsteady laminar boundary layer flow of viscous incompressible fluid over a continuous moving stretching sheet which issue from a thin slot. The coordinate system is such that x-axis is taken along the stretching surface in the direction of the motion with the slot at origin, and the y-axis is perpendicular to the surface of the sheet as shown schematically in Fig.1. A uniform transverse magnetic field $B(x)$ is applied along the y-axis. The surface of the sheet is maintained at uniform temperature and concentration, T_w and C_w, respectively, and these values are assumed to be greater than the ambient temperature and concentration, T_∞ and C_∞, respectively. The flow is assumed to be confined in a region $y > 0$. We consider the non-uniform internal heat generation/absorption in the flow to get the temperature and concentration differences between the surface and the ambient fluid. We assume that the velocity is proportional to its distance from the slit. Under the usual boundary layer approximation, the governing equations describing the momentum, energy and concentration in the presence of radiation, thermophoresis and other important parameters take the following form:

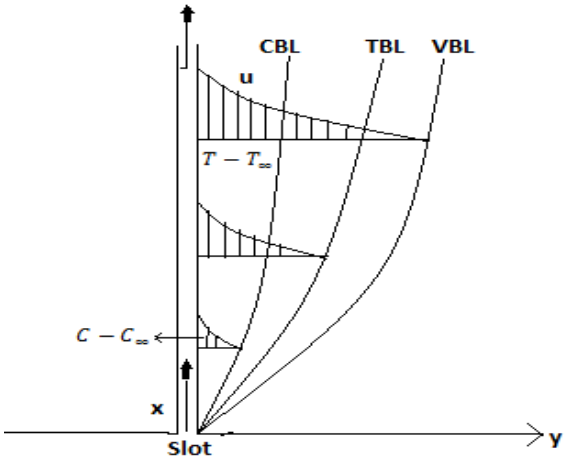

Fig.1. Flow configuration and coordinate system.

$$\frac{\partial u}{\partial x} + \frac{\partial v}{\partial y} = 0 \qquad (1)$$

$$\rho\left(\frac{\partial u}{\partial t} + u\frac{\partial u}{\partial x} + v\frac{\partial u}{\partial y}\right) = \nu\frac{\partial^2 u}{\partial y^2} - \frac{\nu}{k^1}u + \beta_T g(T - T_\infty) + \beta_C g(C - C_\infty) - \sigma {B_0}^2 u \qquad (2)$$

$$\frac{\partial T}{\partial t} + u\frac{\partial T}{\partial x} + v\frac{\partial T}{\partial y} = \frac{\kappa}{\rho c_p}\frac{\partial^2 T}{\partial y^2} - \frac{1}{\rho c_p}\frac{\partial q_r}{\partial y} + \frac{1}{\rho c_p}(q''') + \frac{D_m k_T}{c_s c_p}\frac{\partial^2 C}{\partial y^2} \quad (3)$$

$$\frac{\partial C}{\partial t} + u\frac{\partial C}{\partial x} + v\frac{\partial C}{\partial y} = D_m\frac{\partial^2 C}{\partial y^2} + \frac{D_m k_T}{T_m}\frac{\partial^2 T}{\partial y^2} - \frac{\partial}{\partial y}(V_T C) \quad (4)$$

The associated boundary conditions are

$$u = U_w(x,t),\ v = V_w\ ,\ T = T_w(x,t)\ ,\ C = C_w(x,t), \quad \text{at } y = 0, \quad (5)$$

$$u \to 0,\ T \to T_\infty\ ,\ C \to C_\infty\ , \quad as\ y \to \infty. \quad (6)$$

Where u and v are the components of velocity along x and y directions, respectively and t is the time. T is the temperature and C is the concentration inside the boundary layer, c_p is the specific heat at constant pressure, $c_s$is the concentration susceptibility, ρ is the density of the fluid,κ is the thermal conductivity, v is the kinematic viscosity, μ is the fluid viscosity, $T_w(x,t)$ is the stretching surface temperature, $C_w(x,t)$ is the concentration of the stretching surface, T_∞ is the temperature far away from the stretching surface with $T_w > T_\infty$, C_∞ is the concentration far away from the stretching surface with $C_w > C_\infty$. The term $V_w = -\sqrt{\frac{vU_w}{2x}}f(0)$ represents the mass transfer at the surface with $V_w < 0$ for suction and $V_w > 0$ for injection.

The non-uniform heat source/sink, q''' , is defined as

$$q''' = \frac{\kappa U_w(x,t)}{xv}[A_1(T_w - T_\infty)f' + (T - T_\infty)B_1],$$

Where A_1 and B_1 are the coefficients of space and temperature-dependent heat source/sink, respectively. The case $A_1 > 0\ , B_1 > 0$ corresponds to internal heat source and the case $A_1 < 0\ , B_1 < 0$ corresponds to internal heat sink.

Due to stretching of the sheet the flow is caused and it moves with the surface velocity, temperature and concentration of the form

$$U_w(x,t) = \frac{ax}{1-ct},\ \ T_w(x,t) = T_\infty + \frac{ax}{1-ct}\ , C_w(x,t) = C_\infty + \frac{ax}{1-ct} \quad (7)$$

Where a(stretching rate) and c are positive constants with $ct < 1, c \geq 0$. It is noticed that the stretching rate $\frac{a}{1-ct}$ is increases with time t since $a > 0$.

The following similarity transformations are introduced to simplify the mathematical analysis of the problem

$$\eta = \sqrt{\frac{a}{\nu(1-ct)}}\, y,\ u = \frac{ax}{1-ct} f'(\eta),\ v = -\sqrt{\frac{\nu a}{1-ct}}\, f(\eta), \tag{8}$$

$$\theta(\eta) = \frac{T-T_\infty}{T_w-T_\infty},\ \phi(\eta) = \frac{C-C_\infty}{C_w-C_\infty}. \tag{9}$$

By using Roseland approximation for radiation, the radiative heat flux q_r is defined as

$$q_r = -\frac{4\sigma^*}{3K^*}\frac{\partial T^4}{\partial y}, \tag{10}$$

Where σ^* is the Stephan-Boltzman constant,K^* is the mean absorption coefficient. We assume that the temperature differences within the flow are such that the term T^4 may be expressed as a linear function of temperature. This is accomplished by expanding T^4 in a Taylor series about a free stream temperature T_∞ as follows:

$$T^4 = {T_\infty}^4 + 4{T_\infty}^3(T - T_\infty) + 6{T_\infty}^2(T - T_\infty)^2 + \cdots \tag{11}$$

Neglecting higher-order terms in the above Eq.(11) beyond the first degree in $(T - T_\infty)$, we get

$$T^4 \cong 4{T_\infty}^3 T - 3{T_\infty}^4\ . \tag{12}$$

Thus substituting Eq.(12) in Eq.(10), we get

$$q_r = -\frac{16{T_\infty}^3\sigma^*}{3K^*}\frac{\partial T}{\partial y}. \tag{13}$$

The effect of thermophoresis is usually prescribed by means of an average velocity acquired by small particles to the gas velocity when exposed to a temperature gradient. In boundary layer flow, the temperature gradient in y-direction is very much larger than in the x-direction and therefore only the thermophoretic velocity in y-direction is considered. As a consequence, the thermophoretic velocity V_T, which appears in Eq.(4), is expressed as

$$V_T = -\frac{k_1 \nu}{T_r} \frac{\partial T}{\partial y} \qquad (14)$$

in which k_1 is the thermophoretic coefficient and T_r is the reference temperature. A thermophoretic parameter τ is given by the relation

$$\tau = -\frac{k_1 (T_w - T_\infty)}{T_r} \qquad (15)$$

Where the typical values of τ are 0.01, 0.1and 1.0 corresponding to approximate values of $-k_1(T_w - T_\infty)$ equal to 3, 30, 300K for a reference temperature of *T=300K.*

Substituting Eqs.(8),(9) into Eqs.(2) – (6), we obtain

$$f''' + ff'' - f'^2 - \alpha\left(f' + \frac{1}{2}\eta f''\right) + G(\theta + N\phi) - (M + K)f' = 0 \qquad (16)$$

$$\left(1 + \frac{4}{3}An\right)\theta'' + Pr(f\,\theta' - f'\theta) - Pr\,\alpha\left(\theta + \frac{1}{2}\eta\,\theta'\right) + (A_1 f' + B_1\,\theta) + Du\,\phi'' = 0 \quad (17)$$

$$\phi'' - Sc\,(2\,f'\phi - f\,\phi') - Sc\;\alpha\left(\phi + \frac{1}{2}\eta\,\phi'\right) + Sc\,Sr\,\theta'' - \tau(\theta'\varphi' + \theta''\varphi) = 0 \quad (18)$$

The boundary conditions take the form

$$f = f_w, \quad f' = 1, \quad \theta = 1, \quad \varphi = 1, \qquad at\ \eta = 0, \qquad (19)$$

$$f' = 0, \quad \theta = 0, \quad \varphi = 0, \qquad at\ \eta \to \infty. \qquad (20)$$

Where Pr is the Prandtl number, An is the radiation parameter, α is the unsteadiness parameter, M is the magnetic field parameter, K is the permeability parameter, Sr is the Soret parameter, Du is the Dufour parameter, $\tau$is the thermophoresis parameter, Sc is the Schmidt number,$f(0) = f_w$ with $f_w > 0$ corresponds to suction and $f_w < 0$ represents injection.

Quantities of practical interest in this problem are the local skin friction coefficient C_f, the local Nusselt number Nu_x, and the local Sherwood number Sh_x, are defined as

$$C_f = \frac{\tau_w}{\rho\, U_w^2/2}, Nu_x = \frac{x\, q_w}{\kappa(T_w - T_\infty)}, \; Sh_x = \frac{x\, J_w}{D_m\,(C_w - C_\infty)}.$$

Here τ_w,q_w, and J_w are the wall shear stress, surface heat flux and the mass flux, respectively. Using (8) and (9), we obtain the dimensionless versions of these key design quantities:

$$C_f = \frac{f''(0)}{Re_x^{\frac{1}{2}}}, \quad Nu_x = -\theta'(0)Re_x^{\frac{1}{2}}, \quad Sh_x = -\varphi'(0)Re_x^{\frac{1}{2}}.$$

Since the highly non-linear nature of ordinary differential equations (16)–(18)together with boundary conditions (19)-(20), they cannot be solved analytically. So the variational finite-element method [35,36,37 and 38] has been implemented.

3. NUMERICAL METHOD OF SOLUTION

3.1. The finite-element method

The finite-element method (FEM) is such a powerful method for solving ordinary differential equations and partial differential equations. The basic idea of this method is dividing the whole domain into smaller elements of finite dimensions called finite elements. This method is such a good numerical method in modern engineering analysis, and it can be applied for solving integral equations including heat transfer, fluid mechanics, chemical processing, electrical systems, and many other fields. The steps involved in the finite-element are as follows.

(i) Finite-element discretization

The whole domain is divided into a finite number of sub domains, which is called the discretization of the domain. Each sub domain is called an element. The collection of elements is called the finite-element mesh.

(ii) Generation of the element equations

a. From the mesh, a typical element is isolated and the variational formulation of the given problem over the typical elements constructed.
b. An approximate solution of the variational problem is assumed, and the element equations are made by substituting this solution in the above system.
c. The element matrix, which is called stiffness matrix, is constructed by using the element interpolation functions.

(iii) Assembly of element equations

The algebraic equations so obtained are assembled by imposing the inter element continuity conditions. This yields large number of algebraic equations known as the global finite-element model, which governs the whole domain.

(iv) Imposition of boundary conditions

The essential and natural boundary conditions are imposed on the assembled equations.

(v) Solution of assembled equations

The assembled equations so obtained can be solved by any of the numerical techniques, namely, the Gauss elimination method, LU decomposition method, etc. An important consideration is that of the shape functions which are employed to approximate actual functions.

For the solution of system non-linear ordinary differential equation (16-18) together with boundary conditions (19-20), first we assume that

$$\frac{\partial \mathrm{f}}{\partial \eta} = \mathrm{h} \tag{21}$$

The equations (16) to (18) then reduces to

$$h'' + f h' - h^2 - \alpha\left(h + \frac{1}{2}\eta\, h'\right) - (M + K)\, h = 0 \tag{22}$$

$$\left(1 + \frac{4}{3}An\right)\theta'' + Pr(f\,\theta' - h\,\theta) - Pr\,\alpha\left(\theta + \frac{1}{2}\eta\,\theta'\right) + (A_1\, h + B_1\,\theta) + Du\,\phi'' = 0 \tag{23}$$

$$\phi'' - Sc\,(2\,h - f\,\phi') - Sc\;\alpha\left(\phi + \frac{1}{2}\eta\,\phi'\right) + Sc\,Sr\,\theta'' - \tau(\theta'\varphi' + \theta''\varphi) = 0 \tag{24}$$

The boundary conditions take the form

$$f = f_w, \quad h = 1, \quad \theta = 1, \quad \varphi = 1, \quad at\ \eta = 0, \tag{25}$$

$$h = 0, \quad \theta = 0, \quad \varphi = 0, \quad at\ \eta \to \infty. \tag{26}$$

It has been observed that for large values of $\eta\,(> 6)$, there is no remarkable change in the profiles, so, for computational purpose infinity has been taken as 6.

3.2. Variational formulation

The variational form associated with Eqs. (21) to (24) over a typical linear element (η_e, η_{e+1}) is given by

$$\int_{\eta_e}^{\eta_{e+1}} w_1 \left(\frac{\partial \mathrm{f}}{\partial \eta} - \mathrm{h}\right) \mathrm{d}\eta = 0 \tag{27}$$

$$\int_{\eta_e}^{\eta_{e+1}} w_2 \left(h'' + f h' - h^2 - \alpha\left(h + \frac{1}{2}\eta\, h'\right) - (M + K)\, h\right) \mathrm{d}\eta = 0 \tag{28}$$

$$\int_{\eta_e}^{\eta_{e+1}} w_3 \left(\left(1+\frac{4}{3}An\right)\theta'' + Pr(f\,\theta' - h\,\theta) - \Pr\alpha\left(\theta+\frac{1}{2}\eta\,\theta'\right) + A1\,h + B1\,\theta + Du\,\phi''\right)d\eta = 0 \qquad (29)$$

$$\int_{\eta_e}^{\eta_{e+1}} w_4 \left(\phi'' - Sc\,(2h - f\,\phi') - Sc\;\alpha\left(\phi+\frac{1}{2}\eta\,\phi'\right) + Sc\,Sr\,\theta'' - \tau(\theta'\varphi' + \theta''\varphi)\right)d\eta = 0 \qquad (30)$$

Where w_1, w_2, w_3 and w_4 are arbitrary test functions and may be viewed as the variations in *f*, *h*, θ, and ϕ, respectively.

3.3. Finite- element formulation

The finite-element model may be obtained from above equations by substituting finite-element approximations of the form

$$f = \sum_{j=0}^{2} f_j \Psi_j \;, h = \sum_{j=0}^{2} h_j \Psi_j \;, \qquad \theta = \sum_{j=0}^{2} \theta_j \Psi_j \;, \qquad \phi = \sum_{j=0}^{2} \phi_j \Psi_j \qquad (31)$$

With $w_1 = w_2 = w_3 = w_4 = \Psi_i, \qquad (i = 1,2).$

Where Ψ_i are the shape functions for a typical element (η_e, η_{e+1}) and are defined as

$$\Psi_1^e = \frac{(\eta_{e+1}-\eta)}{(\eta_{e+1}-\eta_e)} \;, \qquad \Psi_2^e = \frac{(\eta-\eta_e)}{(\eta_{e+1}-\eta_e)} \;, \qquad \eta_e \le \eta \le \eta_{e+1}. \qquad (32)$$

The finite element model of the equations thus formed is given by

$$\begin{bmatrix} [K^{11}] & [K^{12}] & [K^{13}] & [K^{14}] \\ [K^{21}] & [K^{22}] & [K^{23}] & [K^{24}] \\ [K^{31}] & [K^{32}] & [K^{33}] & [K^{34}] \\ [K^{41}] & [K^{42}] & [K^{43}] & [K^{44}] \end{bmatrix} \begin{bmatrix} f \\ h \\ \theta \\ \phi \end{bmatrix} = \begin{bmatrix} \{r^1\} \\ \{r^2\} \\ \{r^3\} \\ \{r^4\} \end{bmatrix}$$

Where $[K^{mn}]$ and $[r^m]$ (*m, n = 1, 2, 3, 4*) are defined as

$$K_{ij}{}^{11} = \int_{\eta_e}^{\eta_{e+1}} \Psi_i \frac{\partial \Psi_j}{\partial \eta} d\eta \;, \quad K_{ij}{}^{12} = -\int_{\eta_e}^{\eta_{e+1}} \Psi_i \Psi_j \, d\eta \;,$$

$$K_{ij}{}^{13} = G \int_{\eta_e}^{\eta_{e+1}} \Psi_i (\bar{\theta} + N\bar{\phi}) d\eta, \quad K_{ij}{}^{14} = 0. K_{ij}{}^{21} = \int_{\eta_e}^{\eta_{e+1}} \Psi_i \, \bar{h} \Psi_j \, d\eta$$

$$K_{ij}{}^{22} = \int_{\eta_e}^{\eta_{e+1}} \left\{ -\frac{\partial \Psi_i}{\partial \eta}\frac{\partial \Psi_j}{\partial \eta} - \Psi_i \bar{h} \Psi_j - \alpha \left\{ \Psi_i \Psi_j + \frac{1}{2}\eta \Psi_i \bar{h} \Psi_j \right\} \right\} d\eta - \int_{\eta_e}^{\eta_{e+1}} \Psi_i (M+K) \Psi_j \, d\eta ,$$

$$K_{ij}{}^{23} = 0 \ , K_{ij}{}^{24} = 0 ,$$

$$K_{ij}{}^{31} = Pr \int_{\eta_e}^{\eta_{e+1}} \Psi_i \bar{\theta} \, \Psi_j \, d\eta \, , K_{ij}{}^{32} = -Pr \int_{\eta_e}^{\eta_{e+1}} \Psi_i \, \Psi_j \, d\eta + A_1 \int_{\eta_e}^{\eta_{e+1}} \Psi_i \Psi_j \, d\eta \ ,$$

$$K_{ij}{}^{33} = -\left(1 + \frac{4}{3}An\right) \int_{\eta_e}^{\eta_{e+1}} \frac{\partial \Psi_i}{\partial \eta}\frac{\partial \Psi_j}{\partial \eta} \, d\eta + Pr \, \alpha \int_{\eta_e}^{\eta_{e+1}} \Psi_i (1 + \frac{1}{2}\eta \bar{\theta} + B_1) \Psi_j \, d\eta$$

$$K_{ij}{}^{34} = Du \int_{\eta_e}^{\eta_{e+1}} \frac{\partial \Psi_i}{\partial \eta}\frac{\partial \Psi_j}{\partial \eta} \, d\eta.G$$

$$K_{ij}{}^{41} = Sc \int_{\eta_e}^{\eta_{e+1}} \Psi_i \bar{\phi} \, \Psi_j \, d\eta , \quad K_{ij}{}^{42} = 2 \, Sc \int_{\eta_e}^{\eta_{e+1}} \Psi_i \, \Psi_j \, d\eta , \ ,$$

$$K_{ij}{}^{43} = Sc \, Sr \int_{\eta_e}^{\eta_{e+1}} \frac{\partial \Psi_i}{\partial \eta}\frac{\partial \Psi_j}{\partial \eta} \, d\eta + \mathrm{Sc} \, \alpha \int_{\eta_e}^{\eta_{e+1}} \Psi_i (1 + \frac{1}{2}\eta \bar{\phi}) \Psi_j \, d\eta - \tau \int_{\eta_e}^{\eta_{e+1}} \Psi_i \bar{\phi} \frac{\partial \Psi_j}{\partial \eta} \, d\eta -$$

$\tau \eta e \eta e{+}1 \partial \Psi i \partial \eta \partial \Psi j \partial \eta \, d\eta$, $Kij44 = \eta e \eta e{+}1 \partial \Psi i \partial \eta \partial \Psi j \partial \eta \, d\eta$.

$$r_i^2 = 0 \quad , \ r_i^2 = -\left(\Psi_i \frac{d\Psi_i}{d\eta}\right)_{\eta_e}^{\eta_{e+1}} \ , \ r_i^3 = -\left(\Psi_i \frac{d\Psi_i}{d\eta}\right)_{\eta_e}^{\eta_{e+1}} \ , \ r_i^4 = -\left(\Psi_i \frac{d\Psi_i}{d\eta}\right)_{\eta_e}^{\eta_{e+1}}$$

Where

$$\bar{f} = \sum_{j=0}^{2} f_i \frac{\partial \Psi_i}{\partial \eta} \bar{h} = \sum_{j=0}^{2} h_i \frac{\partial \Psi_i}{\partial \eta} , \qquad \bar{\theta} = \sum_{j=0}^{2} \theta_i \frac{\partial \Psi_i}{\partial \eta}, \qquad \bar{\phi} = \sum_{j=0}^{2} \phi_i \frac{\partial \Psi_i}{\partial \eta}.$$

After assembly of element equations, we get the system of strongly non-linear equations and are solved using a robust iterative scheme. The system is linearized by incorporating the functions $\bar{f}, \bar{h}, \bar{\theta}$ and $\bar{\phi}$, which are assumed to be known. After imposing the boundary conditions, we get the less number of non-linear equations and are solved using Gauss elimination method by maintaining an accuracy of 0.00001. The computer program of the algorithm was executed in Mathematica 10.0 software.

4. RESULTS AND DISCUSSION

Comprehensive numerical computations were conducted for different values of the parameters that describe the flow characteristics, and the results are illustrated graphically and in tabular form. Selected graphical profiles are presented in Figs. 2 - 27. The Comparison of skin friction coefficient $f''(0)$ for various values of (*Pr)*with [33]is made and the results are shown in Table 1in the absence of the other parameters. The results are also compared for Nusselt number $-\theta'(0)$ for various values of (*Pr*) and α with those of [33, 39, 40]and are presented in Table 2. Thus, it is seen from Tables 1 and 2 that the numerical results are in close agreement with those published previously.

The influence of magnetic field parameter (*M*) on velocity and temperature profiles in the boundary layer is depicted in Fig.2 - 4. It is noticed from this figure that momentum boundary layer thickness decreases and thermal boundary layer thickness depreciates with enhance in the values of (*M*). This is because of the fact that, the presence of magnetic field in an electrically conducting fluid produces a force called Lorentz force, this force acts against the flow direction causes the depreciation in velocity profiles in the flow field (fig 2). We noticed from fig. 3 and fig.4 that temperature and concentration profiles are enhanced with increasing values of M. This is from the reality that, to overcome the drag force imposed by the Lorentzian retardation the fluid has to perform extra work; this supplementary work can be converted into thermal energy which increases the thermal and solutal boundary layer thickness of the fluid.

Figures 5 - 7 depict velocity (f') , temperature (θ) and concentration (φ) distributions for different values of the suction parameter (f_w). From these figures, it can be seen that as suction parameter (f_w) increases the fluid velocity, temperature and concentration profiles decreases. This is due to the fact that the suction is taken away the warm fluid from the surface of the sheet and thereby decreases the thickness of the velocity boundary layer(Fig.5). Fig.6 shows the effect of the suction parameter on the temperature profiles. It is observed that an increase in (f_w) decreases the temperature profiles in the flow region. This is because of the fact that as suction is increased, more warm fluid is taken away from the fluid region causes depreciation in thermal boundary layer thickness. We noticed from Fig.7 that the concentration profiles decelerates with increase in suction parameter, this is because of suction stabilizes the growth of the solutal boundary layer thickness.

The influence of unsteadiness parameter (α) on the temperature, and concentration profiles is depicted in figures 8- 9. It can be seen that temperature profiles decelerates with increase in the values of unsteadiness parameter (α). This is because of the usual fact that, the motion is generated by the stretching of the sheet and the stretching sheet velocity and temperature is greater than the free stream velocity and temperature, so, the thermal boundary layer thickness decreases with increase in the values of α as shown in Fig8.The concentration profiles also decreases in the flow region and is shown in Fig.9. It is also observed that temperature profiles decreases smoothly in the absence of unsteadiness parameter (α=0) whereas temperature profiles continuously decreases with the increasing values of unsteadiness parameter. This shows that the rate of cooling is much faster for the higher values of unsteadiness parameter and it takes longer time for cooling in the steady flows.

The impact of porous parameter (K) on velocity and temperature profiles is shown in Figs. 10 and 11. It is noticed that the velocity decelerates with the higher values of porous parameter(K). This is because of the fact that, the porosity parameter in depending on the permeability parameter (K), the values of porosity parameter increases means the values of permeability parameter decreases causes the depreciation in the velocity profiles (fig.10). However, the temperature profiles of the fluid rises as the values porous parameter (K) increases. This is because of the fact that the thickness of the thermal boundary layer enhance with the higher values of (K).

The effect of thermophoretic parameter(τ) on temperature and concentration profiles is plotted in Figs. 12 and 13. It is seen form Fig.12 that an increase in (τ) there exist slight enhance in the temperature profiles throughout the flow regime. This is because of the fact that the particles near the hot surface create a thermophoretic force.Fig.13 exhibits the impact of (τ) on concentration profiles, it is noticed that concentration profiles decreases with increase in thermophoretic parameter (τ).This is because, the fluid moves from hot surface to the cold surface, then the values of thermophoretic parameter have been taken positive. From these two figures we conclude that the imposition of thermophoretic particle deposition into the flow increases the thickness of thermal boundary layer and decreases the solutal boundary layer thickness.

Temperature and concentration profiles for different values of space dependent and temperature-dependent coefficients ($A1$) and ($B1$) for heat source/sink are depicted in Figs.14

to17.It is observed that temperature in thermal boundary layer increases with increase in (*A1*)and (*B1*)(positive values), whereas thermal boundary layer thickness decelerates with decrease in heat absorption parameters(*A1*)and(*B1*) (negative values). This is due to the fact that, with an increase in A1>0, B1>0(heat source) the boundary layer creates energy which causes the rise in temperature profiles, whereas, with decrease in A1< 0, B1< 0(heat absorption) the boundary layer absorbs the energy so that the thermal boundary layer thickness decreases in the fluid regime as shown in Figs.14 and 16. Exact reverse trend is noticed on concentration profiles with space dependent and temperature-dependent coefficients (*A1*) and (*B1*) for both heat generation and heat absorption cases; this is plotted in Figures 15 and 17.

The combined effects of Thermo-Diffusion(Soret) and Diffusion-Thermo (Dufour) on temperature and concentration profiles are plotted in Figs.18 and 19.The values of *Sr* and *Du* have been taken as *Sr* = 1.0, 0.7,0.4,0.1 and *Du* = 0.1, 0.3, 0.5,0.7, i.e. Soret parameter values decreases and Dufour parameter values increases. It is seen from this figures that temperature profiles increases, whereas concentration profiles decelerates with enhance in *Du* and fall in *Sr*. From the definition, Soret number can be defined as the effect of temperature on concentration and Dufour effect can be defined as the effect of concentration on temperature. This shows that, diffusive species with lower Soret values decelerates the concentration profiles whereas temperature species with higher Dufour values has the tendency of increasing the temperature profiles. It is worth noticed that both heat and mass transfer are highly influenced by the *Sr* and *Du*.

Figs. 20 and 21 is the plot of thermal radiation parameter (*An*) on temperature and concentration distributions. It is observed form fig 20 that asthe values of (*An*) increases the thickness of the thermal boundary layer also increases. This is due to thefact that imposition of (*An*)in fluid flow implies increasing of thermal radiation in the thermal boundary layer which results in increase in the value of the temperature profile in the fluid regime. Whereas the reverse trend is observed in solutal boundary layer thickness with increasing values of (*An*) in the flow region and is shown in figure 21.

The temperature and concentration distributions for various values of the Prandtl number (*Pr*) are revealed in Figs. 22 and 23, respectively. It is noticed from fig.22 that the temperature profiles retards in the entire boundary layer regime with the increasing values of Prandtl number (*Pr*). This is because of the fact that, Prandtl number is demarcated as the ratio of the momentum diffusivity to the thermal diffusivity. Increasing the values of (*Pr*) means, the value of thermal

diffusivity is less than the value of momentum diffusivity, which causes the deterioration in the thermal boundary layer thickness (Fig.22). However, the solutal boundary layer thickness is improved in the boundary layer regime as the values of (*Pr*) increases (Fig. 23).

Figure 24 illustrates the effect of Schmidt number (*Sc*) on the concentration distributions in the boundary layer regime. We see from this figure that the concentration profiles are highly influenced and are retards with the higher values of Schmidt number (*Sc*) in the flow region.

The impact of (*G*) on velocity, temperature and concentration profiles is depicted in Fig. 25-27 in the boundary layer regime. It is noticed from fig.25 that the hydrodynamic boundary layer thickness is elevated with the improving values of (*G*). The temperature profiles decelerate in the entire boundary layer region with higher values of G. This is because of the fact that the thermal boundary layer thickness decreases with the increasing values of *G*, as a result the temperature of the fluid decreases (Fig.26). Further, as the value of (*G*) raises the solutal boundary layer thickness depreciates in the boundary layer region (Fig.27).

The variation of local skin-friction co-efficient $(f''(0))$, local Nusselt number $(-\theta'(0))$,and local Sherwood number $-\phi'(0)$ for different values of magnetic parameter (*M*) and suction parameter $(f_w > 0)$are presented inTable 3. It is evident that all these non-dimensional rate coefficients decelerate with increasing values of magnetic parameter M. Further , it is noted that the rates of velocity depreciates, whereas rates of dimensionless heat transfer and rates of dimensionless mass transfer enhances with the increasing values of suction $(f_w > 0)$ parameter.

Influence of space - dependent heat source/sink (*A1*) and temperature-dependent heat source/sink (*B1*) on Skin-friction co - efficient$(f''(0))$, Nusselt number $(-\theta'(0))$ and Sherwood number $(-\phi'(0))$ are presented in table 4.It is observed from this table that the effect of space dependent (*A1*) and temperature-dependent (*B1*) parameters is similar on these non-dimensional rate coefficients. Moreover, rates of non-dimensional velocity and heat transfer decreases whereas rates of non-dimensional mass transfer enhances for the values of both (*A1*) and (*B1*).

The effect of Soret parameter (*Sr*) together with Dufour parameter (*Du*) on these non-dimensional rate coefficients is shown table 5and is observed that $f''(0)$ and $-\theta'(0)$ decelerates, whereas $-\phi'(0)$ enhances in the flow region.

The influence of thermophoretic parameter(τ) and thermal radiation parameter (*An*)on Skin-friction coefficient $(f''(0))$, Nusselt number $(-\theta'(0))$ and Sherwood number $(-\phi'(0))$ is

presented in table 5. It can be noted that local skin-friction coefficient and local Sherwood number increases whereas Nusselt number decreases with the increasing values of (τ) and (*An*).

Table 2.Comparison of $f''(0)$ with previously published data for *k=0, M=0, Sr=0, Du=0, Sc=0, A_1=0, B_1=0, f_w =0 and* $\tau = 0$.

$f''(0)$		
α	Dulal pal [33]	Present Study
0.8	-1.261043	-1.261036
1.2	-1.377724	-1.377658
2.0	-1.587366	-1.587301

Table 3.Comparison of $-\theta'(0)$ with previously published data for *k=0, M=0, Sr=0, Du=0, Sc=0, A_1=0, B_1=0, and* $\tau = 0$.

Nu_x						
α	f_w	Pr	Ishak.A.et.al[39]	Dulal Pal. [33]	Haile.E.et al[40]	Present Study
0.0	0.0	1.0	1.0000	1.0000	1.0004	1.0002
0.0	0.0	3.0	1.9237	1.9236	1.9234	1.9235
0.0	0.0	10.0	3.7207	3.7207	3.7205	3.7205
0.0	0.0	100	12.2941	12.2940	12.2962	12.2948

Table 1:Grid-invariance test for velocity distribution (f'), temperature distribution (θ) and concentration distribution (ϕ) with, *k* = 0.1, *M* = 0.5, f_w= 0.5, α = 0.5, Pr = 0.72, *Sr* =1.0, *Du* = 0.1, *Sc* = 1.0, A_1= - 0.1, B_1 = - 0.1,τ =0.5, An = 0.1.

η	f'				θ				ϕ			
	Step size (*h*)											
	0.04	0.02	0.01	0.005	0.04	0.02	0.01	0.005	0.04	0.02	0.01	0.005
0.0	1.0000	1.0000	1.0000	1.0000	1.0000	1.0000	1.0000	1.0000	1.0000	1.0000	1.0000	1.0000
1.0	0.2474	0.2412	0.2381	0.2380	0.4091	0.4112	0.4120	0.4121	0.3336	0.3340	0.3345	0.3344
2.0	0.0749	0.0731	0.0718	0.0718	0.1965	0.1985	0.1992	0.1993	0.1773	0.1782	0.1784	0.1785
3.0	0.0254	0.0240	0.0237	0.0237	0.1019	0.1031	0.1038	0.1038	0.0857	0.0861	0.0863	0.0863
4.0	0.0000	0.0000	0.0000	0.0000	0.0534	0.0543	0.0546	0.0546	0.0426	0.0430	0.0432	0.0432
5.0	----	----	----	----	0.0264	0.0272	0.0281	0.0281	0.0089	0.0102	0.0104	0.0104
6.0	----	----	----	----	0.0000	0.0000	0.0000	0.0000	0.0000	0.0000	0.0000	0.0000

Table 4: Influence of Magnetic parameter (M) and Suction/Injection parameter (f_w) on Skin-friction co-efficient $(f''(0))$, Nusselt number $(-\theta'(0))$ and Sherwood number $(-\phi'(0))$ for fixed values of *k* = 0.1, α = 0.5, Pr = 0.72,*Sr* =1.0, *Du* = 0.1, *Sc* = 1.0, A_1 = - 0.1, B_1= - 0.1, τ =0.5, An = 0.1.

Parameter		$f''(0)$	$-\theta'(0)$	$-\phi'(0)$
M	f_w			
0.1	0.5	1.515874	1.095458	1.435307
0.5	0.5	-1.666644	1.076938	1.404446
1.0	0.5	-1.834613	1.058171	1.372403
1.5	0.5	-1.986079	1.042780	1.345560
0.5	0.1	-1.451998	1.955840	1.278779
0.5	0.3	-1.555748	1.014205	1.339800
0.5	0.5	-1.666644	1.076938	1.404446
0.5	0.7	-1.784578	1.144081	1.473173

Table 5: Influence of space - dependent heat source/sink (A_1) and temperature-dependent heat source/sink (B_1) on Skin-friction coefficient $(f''(0))$, Nusselt number $(-\theta'(0))$ and Sherwood number $(-\phi'(0))$ for fixed values of k = 0.1, M = 0.5, f_w= 0.5, α = 0.5, Pr = 0.72, Sr =1.0, Du = 0.1, Sc = 1.0, τ =0.5, An = 0.1.

Parameter		$f''(0)$	$-\theta'(0)$	$-\phi'(0)$
A1	B1			
-0.5	-0.1	-1.336331	1.063821	1.098906
-0.1	-0.1	-1.325783	0.848838	1.259929
0.1	-0.1	-1.370402	0.741372	1.340362
0.5	-0.1	-1.402364	0.580215	1.460915
-0.1	-0.3	-1.127874	0.927363	1.204698
-0.1	-0.1	-1.257839	0.848835	1.259929
-0.1	0.1	-1.659464	0.761911	1.319952
-0.1	0.2	-1.786872	0.663112	1.386590

Table 6: Combined impact of Soret effect (Sr) and Dufour effect (Du) on Skin-friction coefficient $(f''(0))$, Nusselt number $(-\theta'(0))$ and Sherwood number $(-\phi'(0))$ for fixed values of k = 0.1, M = 0.5, f_w= 0.5, α = 0.5, Pr = 0.72, A_1 = - 0.1, B_1 = - 0.1, Sc = 1.0, τ =0.5, An = 0.1.

Parameter		$f''(0)$	$-\theta'(0)$	$-\phi'(0)$
Sr	Du			
1.0	0.1	-1.286738	1.096435	1.073863
0.7	0.3	-1.318896	0.954126	1.344509
0.4	0.5	-1.374805	0.767018	1.555324
0.1	0.7	-1.354916	0.572113	1.672064

Table 7: Impact of Thermophoretic parameter (τ) and Radiation parameter (An) on Skin-friction coefficient $(f''(0))$, Nusselt number $(-\theta'(0))$ and Sherwood number $(-\phi'(0))$ for fixed values of k = 0.1, M = 0.5, f_w= 0.5, α = 0.5, Pr = 0.72, A_1 = - 0.1, B_1 = - 0.1, Sc = 1.0, Sr =1.0, Du = 0.1.

Parameter		$f''(0)$	$-\theta'(0)$	$-\phi'(0)$
Sr	Du			
0.1	0.1	-1.325783	0.848835	1.259929
0.3	0.1	-1.320339	0.805255	1.405978
0.5	0.1	-1.234173	0.766189	1.537093
0.7	0.1	-1.212000	0.730941	1.655567
0.5	0.1	-1.286738	1.096735	1.073863
0.5	0.3	-1.269317	0.977259	1.158216
0.5	0.5	-1.245810	0.886694	1.220849
0.5	0.7	-1.226764	0.815356	1.269324

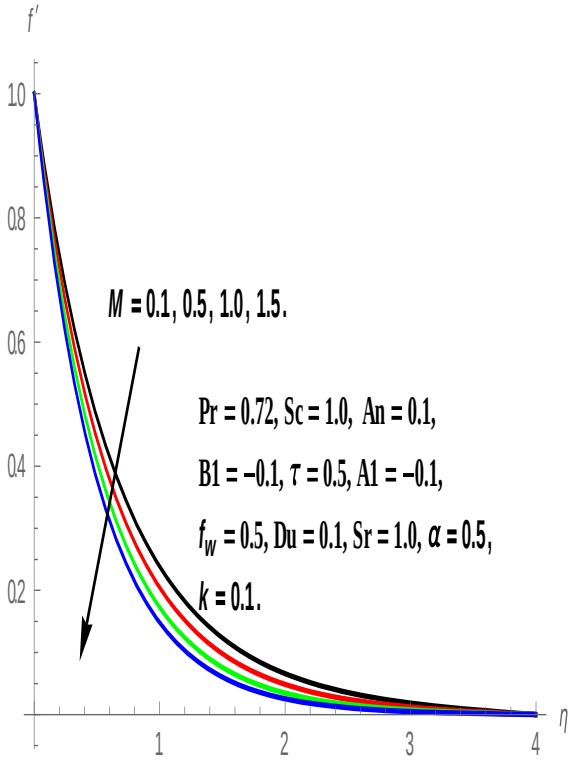

Fig. 2.Effect of M on Velocity profile

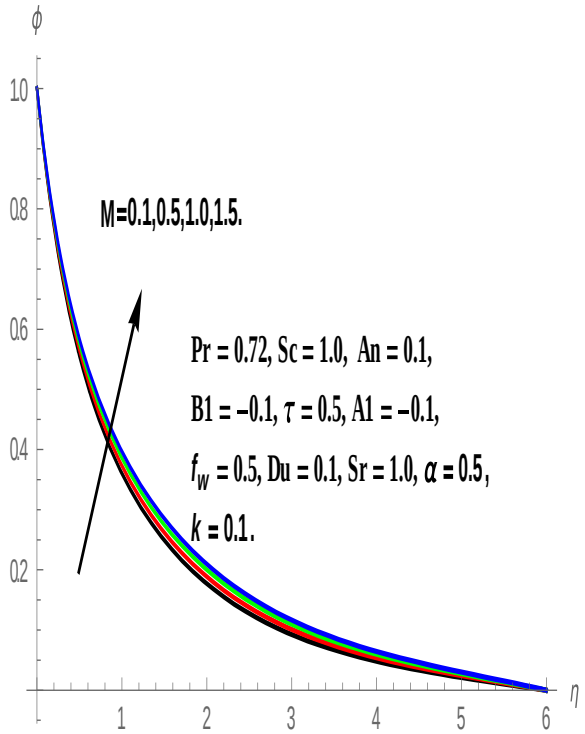

Fig. 3.Effect of M on temperature profile.

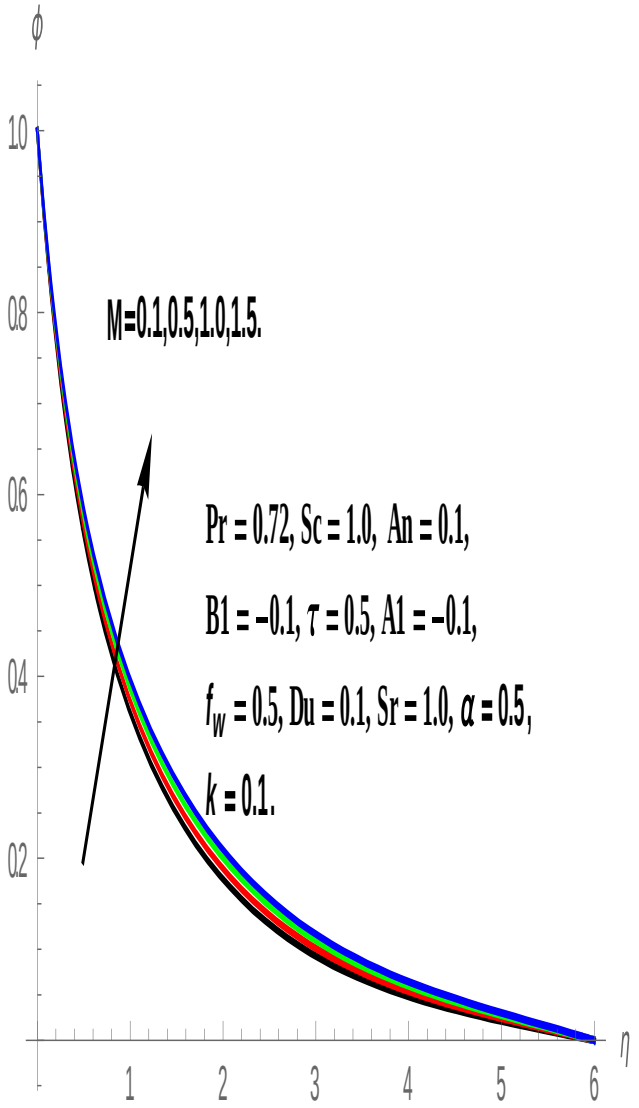

Fig.4.Effect of M on Concentration profile

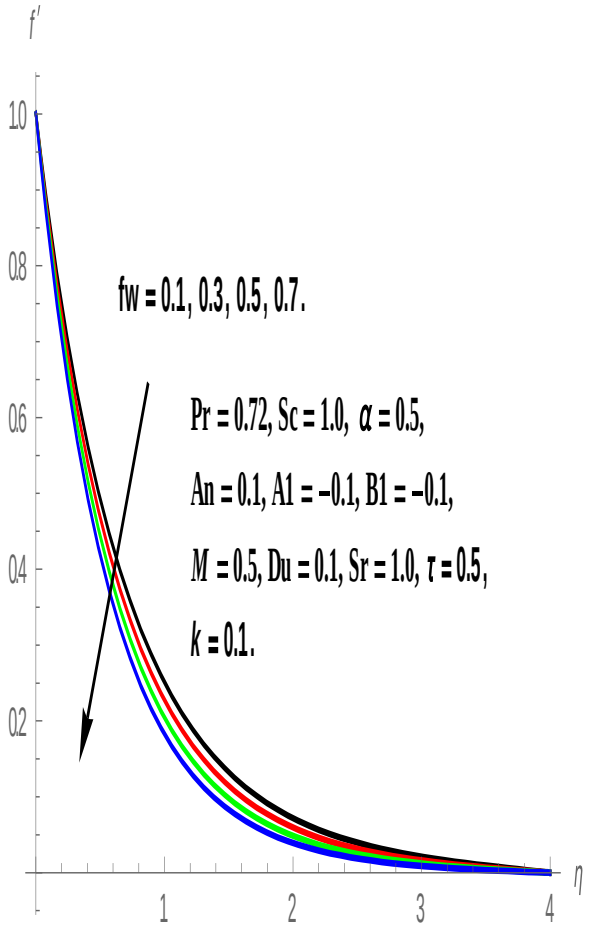

Fig. 5.Effect of f_w on Velocity profile.

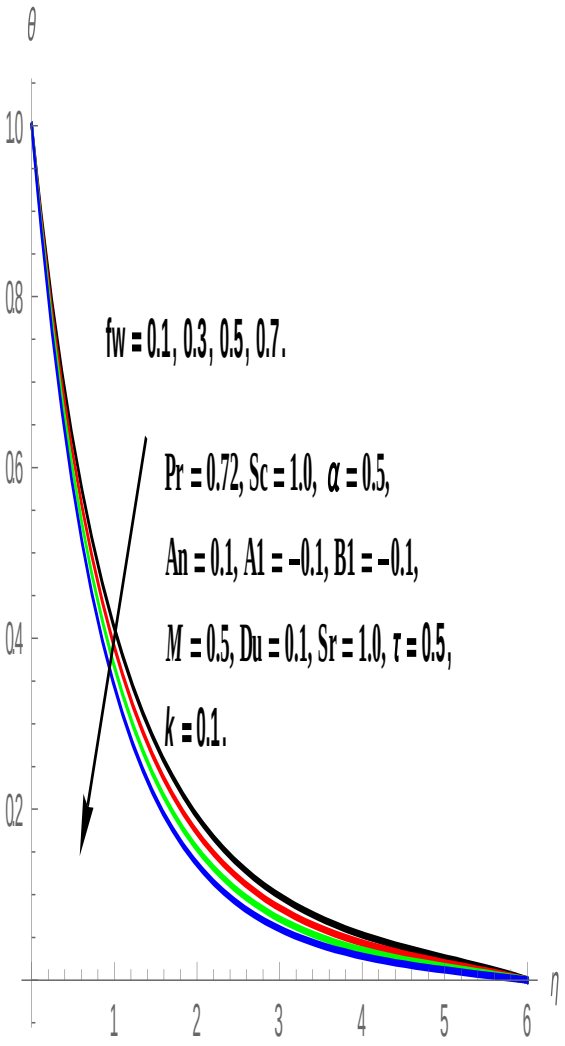

Fig. 6.Effect of f_w on Temperature profile.

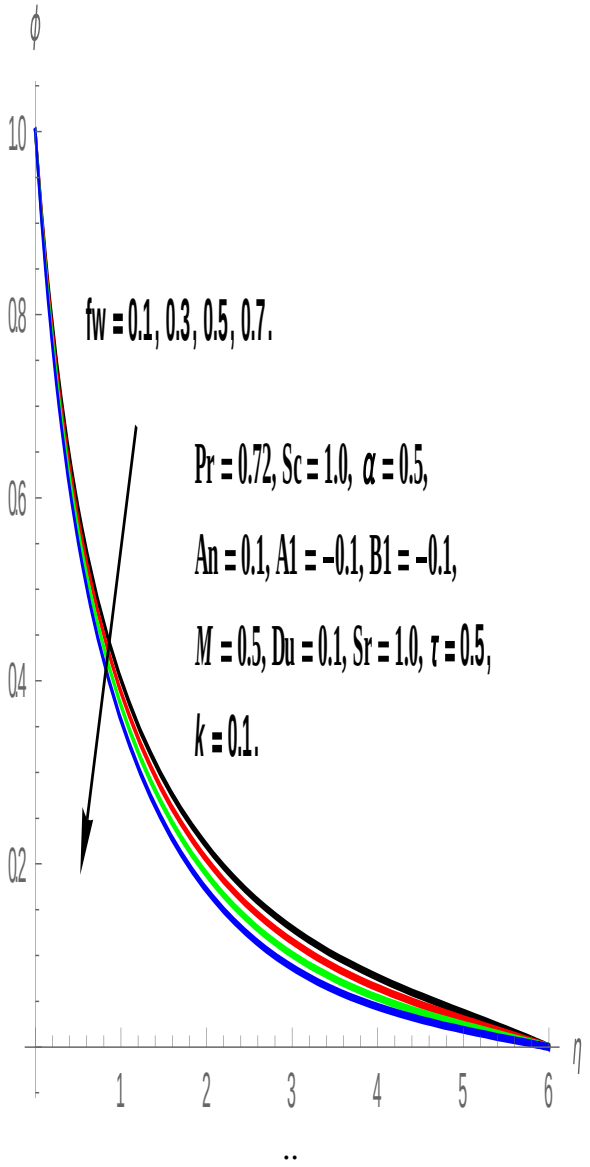

Fig. 7.Effect of f_w on Concentration profile

..

REFERENCES:

[1] Sakiadis B.C, Boundary layer behavior on continuous solid surfaces, AIChE J.7, 26–28, 1961.

[2] Tsou F.K, Sparrow E.M, and Goldstein R.J., Flow and heat transfer in the boundary layer on a continuous moving surface, Int. J. Heat Mass Transfer 10, 219–235, 1967.

[3] Crane L.J, Flow past a stretching plate, Z. Angew. Math. Phys, 21,645–647,1970.

[4] Gupta P.S, and Gupta A.S, Heat and mass transfer on a stretching sheet with suction or blowing, Can. J. Chem. Eng, 55, 744–746, 1977.

[5] Grubka L.G, and Bobba K.M, Heat transfer characteristics of a continuous stretching surface with variable temperature, J. Heat Transfer — Trans. ASME107 (1985) 248–250.

[6] Ali M.E, Heat transfer characteristics of a continuous stretching surface, Heat Mass Transfer 29, 227–234, 1994.

[7] Vajravelu K., Flow and heat transfer in a saturated porous medium over a stretching surface, Z. Angew. Math. Mech, 74, 605–614, 1994.

[8] PlumbO.A, Huenfeld J.S, and Eschbach E.J, The effect of cross flow and radiation on natural convection from vertical heated surfaces in saturated porous media, in: AIAA 16th Thermophysics Conference, June 23–25, Palo Alto, California, USA, 1981.

[9] Pal D, and Mandal H, The influence of thermal radiation on hydromagnetic Darcy–Forchheimer mixed convection flow past a stretching sheet embedded in a porous medium, Meccanica, doi:10.1007/s 11012-010-9334-8, 2010.

[10] Mansour M.A, and El-Shaer N.A, Radiative effects on magnetohydrodynamic natural convection flows saturated in porous media, J. Magn. Magn. Mater, 237, 327–341, 2001.

[11] Pal D, Heat and mass transfer in stagnation-point flow towards a stretching surface in the presence of buoyancy force and thermal radiation, Meccanica, 44,145–158,2005.

[12] Vajravelu K, and Rollins D, Heat transfer in electrically conducting fluid over a stretching surface, Internat. J. Non-Linear Mech, 27 (2), 265–277, 1992.

[13] Molla Md.M, Saha S.C, and Hossain Md.A, Radiation effect on free convection laminar flow along a vertical flat plate with stream wise sinusoidal surface temperature, Math. Comput. Modeling, 53,1310–1319, 2011.

[14] Abo-Eldahab E.M, and El-Gendy M.S, Heat current and Ohmic heating effect on mixed convection boundary layer flow of a micropolar fluid from a rotating cone with power-law variation in surface temperature, Int. Commun. Heat Mass Transfer , 31,751–762, 2004.

[15] Talbot L, Cheng R.K, Schefer R.W, and et al, Thermophoresis of particles in a heated boundary layer. J. Fluid Mech,101(4), 737–758,1980.

[16] Duwairi H.M, Damseh R.A, Effect of thermophoresis particle deposition on mixed convection from vertical surfaces embedded in saturated porous medium, Int. J. Numerical Methods Heat Fluid Flow,18(2), 202-216,2008.

[17] Damseh R.A, Tahat M.S, and Benim A.C,Non-similar solutions of magnetohydrodynamic and thermophoresis particle deposition on mixed convection problem in porous media along a

verticalsurface with variable wall temperature, Progress in Computational Fluid Dynamics 9(1), 58-65,2009.

[18] Mahdy A, Hady F.M, Effect of thermophoretic particle deposition in non-Newtonian free convection flow over a vertical plate with magnetic field effect, Journal of Non-Newtonian Fluid Mechanics,161(1-3), 37-41,2009.

[19] Liu Z, Chen Z, and Shi M, Thermophoresis of particles in aqueous solution in micro-channel. Applied Thermal Engineering,29(5-6), 1020–1025, 2009.

[20] Postelnicu A, Effects of thermophoresis particle deposition in free convection boundary layer from a horizontal flat plate embedded in a porous medium, Int. J. Heat Mass Transfer 50(15-16), 2981–2985, 2007.

[21] Dinesh K.K, and Jayaraj S, Augmentation of thermophoretic deposition in natural convection flow through a parallel plate channel with heat sources. Int. Communications Heat and Mass Transfer 36, 931–935,2009.

[22] Grosan T, Pop R, and Pop I, Thermophoretic deposition of particles in fully developed mixed convection flow in a parallel plate vertical channel, Heat Mass Transfer 45, 503–509, 2009.

[23] Tsai R, and Huang J.S, Combined effects of thermophoresis and electrophoresis on particle deposition onto a vertical flat plate from mixed convection flow through a porous medium. Chemical Eng. J. 157, 52–59, 2010.

[24] Dulal Pal, and Mondal.H, MHD non-Darcian mixed convection heat and mass transfer over a non-linear stretching sheet with Soret and Dufour effects and chemical reaction, International communications in heat and mass transfer, 463-467,2011.

[25] Makinde, O.D, On MHD Mixed Convection with Soret and Dufour Effects Past a Vertical Plate Embedded in a Porous Medium, Latin American Applied Research 41, 63-68,2011.

[26] P.S. Reddy, and Rao V P: Thermo-Diffusion and Diffusion –Thermo Effects on Convective Heat and Mass Transfer through a Porous Medium in a Circular Cylindrical Annulus with Quadratic Density Temperature Variation – Finite Element Study, **J**ournal of **A**pplied **F**luid **M**echanics,5(4), 139-144, 2012.

[27] Chamkha A.J,and Rashad A.M, Unsteady heat and mass transfer by MHD mixed convection flow from a rotating vertical cone with chemical reaction and Soret and Dufour effects, The Canadian Journal of Chemical Engineering, DOI 10.1002/cjce.21894, 2014.

[28] Wang CY: Liquid film on an unsteady stretching surface, Q Appl Math,48,601–10, 1990.

[29] Elbashbeshy EMA, and Bazid MAA, Heat transfer over an unsteady stretching surface, Heat Mass Transfer,41,1–4, 2004.

[30] Tsai R, Huang K. H, and Huang J. S, Flow and heat transfer over an unsteady stretching surface with non-uniform heat source,Int. Commun. Heat Mass Transfer, 35,1340-1343,2008.

[31] Ishak A, Nazar R, and Pop I, Heat transfer over an unsteady stretching permeable surface with prescribed wall temperature, Nonlinear Anal: Real World Appl,10,2909–13, 2009.

[32] Ishak A, UnsteadyMHD flow and heat transfer over a stretching plate,J. Applied Sci, 10(18), 2127-2131,2010.

[33] Dulal pal, Combined effects of non-uniform heat source/sink and thermal radiation on heat transfer over an unsteady stretching permeable surface, Commun Nonlinear SciNumer Simulat,16, 1890–1904, 2011.

[34] Dulal Pal, HiranmoyMondal,MHD non-Darcian mixed convection heat and mass transfer over a non-linearstretching sheet with Soret–Dufour effects and chemical reaction, International Communications in Heat and Mass Transfer 38, 463–467, 2011.

[35] Bhargava R, Sharma R, and Bég O.A, Oscillatory chemically-reacting MHD free convection heat and mass transfer in a porous medium with Soret and Dufour effects, finite element modeling, Int. J. Appl. Math. Mech, 5 (6),15–37, 2009.

[36] Anwar Bég O, Takhar H.S, Bhargava R, Rawat S, and Prasad V.R, Numerical study of heat transfer of a third grade viscoelastic fluid in non-Darcian porous media with thermo physical effects, Phys. Scr,77, 1–11,2008.

[37] Reddy J.N, An Introduction to the Finite Element Method, McGraw-Hill Book Co., New York, 1985.

[38] Rana P, and Bhargava R, Flow and heat transfer of a Nano fluid over a nonlinearly stretching sheet: a numerical study, Comm. Nonlinear Sci. Numer. Simulat, 17, 212–226, 2012.

[39] Ishak. A, R. Nazar, and I. Pop, Boundary layer flow and heat transfer over an unsteady stretching vertical surface, Meccanica, 44, 369–375, 2009.

[40] Eshetu Haile, and Shankar B, Heat and Mass Transfer in the Boundary Layer of Unsteady Viscous Nano fluid along a Vertical Stretching Sheet, Journal of Computational Engineering, DOI/10.1155/2014/345153, 2014.